Robust Landing and Sliding Maneuver Hybrid Controller for a Quadrotor Vehicle

David Cabecinhas, Roberto Naldi, Carlos Silvestre, Rita Cunha, and Lorenzo Marconi

***Abstract*— This paper addresses the design and experimental evaluation of a robust controller for a quadrotor landing maneuver comprising the approach to a landing slope and sliding on that slope, before coming to a complete halt. During the critical landing flight phase, the dynamics of the vehicle change with the type of contact with the ground, and a hybrid automaton, whose states reflect the several dynamic behaviors of the quadrotor, is employed to model the vehicle throughout the complete maneuver. The quadrotor landing problem is broken down as separate maneuver generation and robust trajectory tracking problems, which are combined to achieve a successful maneuver that is robust to possible uncertainties. The experimental results are provided to attest to the feasibility of the proposed landing procedure.**

***Index Terms*— Landing, quadrotor, robust maneuver, robust trajectory tracking, unmanned aerial vehicle (UAV).**

I. Introduction

FLIGHT control of unmanned aerial vehicles (UAVs) is an active and challenging topic of research, with crucial importance to numerous civilian and military applications. Examples of applications can be gathered from a number of recent journal special issues dedicated to these platforms, with topics ranging from flight control [1] and aerial robotics [2]–[5] to a plethora of remote sensing applications, such as the ones detailed in [6] and [7]. Vertical takeoff and landing rotorcraft, with hover flight capabilities, form a large and important class of UAVs. From this class, we highlight the quadrotor as an ideal platform for robotic systems, particularly suited for the development and test of new control strategies due to its simplicity, high maneuverability, and ability to hover.

Research on autonomous UAVs has been traditionally focused on the free flight (FF) regime and, by now, control of rotorcraft in this flight mode is a thoroughly studied problem for which several solutions have been proposed in [8]. However, in many envisaged working scenarios, an aerial vehicle must also perform challenging takeoff and landing maneuvers, where the vehicle is in contact with the ground and additional complications arise.

The traditional approach to landing a rotorcraft can be divided into three phases: hover, horizontal approach or vertical descent, and settling, which covers the time between the first contact and a full stop of the vehicle [9]. During the landing maneuver, there are two undesirable behaviors arising from the modified dynamics due to contact with the ground, which must be avoided. The first is dynamic rollover, in which the vehicle rolls or pivots around the initial contact point and overturns, if a critical rollover angle is exceeded, precluding the possibility of recovery regardless of the actuation. The dynamic rollover situation is quite dangerous since the vehicle's fast rotating propellers can hit the ground and cause serious damages and, ultimately, vehicle destruction. The second undesirable behavior is a strong impact resulting from shutting off the motors and abruptly hitting the ground on the settling phase. The roll momentum can make the vehicle rock and continue rolling down the landing slope [10]. An impact with a large roll velocity should also be avoided as it can damage the vehicle, its sensors, and its payload.

Contact with the ground, although in general avoided by aerial vehicles, can be particularly helpful for inspection and data acquisition tasks performed with sensors that require close proximity with the ground. A practical application of contact is the cleaning of solar panels and large flat surfaces typically located at a height, which can be performed by a quadrotor sliding on the panel surface. Other surfaces where landing and sliding is feasible are rooftops in otherwise inaccessible buildings and structures. Finally, the proposed landing procedure allows for controlled landing on a wider

Manuscript received January 5, 2014; revised October 26, 2014 and March 9, 2015; accepted June 27, 2015. Date of publication September 4, 2015; date of current version February 17, 2016. Manuscript received in final form July 4, 2015. This work was supported in part by the University of Macau, Macao, China, under Project MYRG2015-00126-FST, in part by the Macao Science and Technology Development Fund under Grant FDCT/048/2014/A1, and in part by the Fundação para a Ciência e a Tecnologia under Project FCT [UID/EEA/50009/2013]. The work of R. Naldi and L. Marconi was supported in part by the European Commission through the SHERPA Project under Grant ICT 600958. The work of R. Cunha was supported by the FCT Investigator Programme under Contract IF/00921/2013. Recommended by Associate Editor K. Morgansen.

D. Cabecinhas is with the Department of Electrical and Computer Engineering, Faculty of Science and Technology, University of Macau, Macao, China, and also with the Laboratory of Robotics and Systems in Engineering and Science (LARSyS), Institute for Systems and Robotics/Instituto Superior Técnico, Lisboa 1049-001 Portugal (e-mail: dcabecinhas@umac.mo).

R. Naldi and L. Marconi are with the Center for Complex Automated Systems, Department of Electronics, Computer Science and Systems, University of Bologna, Bologna 40126, Italy (e-mail: roberto.naldi@unibo.it; lorenzo.marconi@unibo.it).

C. Silvestre is with the Department of Electrical and Computer Engineering, Faculty of Science and Technology, University of Macau, Macao, China. He is on leave from Instituto Superior Técnico, University of Lisbon, 1049-001 Lisbon, Portugal.

R. Cunha is with the Department of Electrical and Computer Engineering, and the Laboratory of Robotics and Systems in Engineering and Science (LARSyS), Institute for Systems and Robotics/Instituto Superior Técnico, Universidade de Lisboa, Lisboa 1049-001, Portugal (e-mail: rita@isr.ist.utl.pt).

Color versions of one or more of the figures in this paper are available online at http://ieeexplore.ieee.org.

Digital Object Identifier 10.1109/TCST.2015.2454445

range of surfaces, such as a mountainous slope, since rocking and rollover of the vehicle are actively avoided, even if sliding is disallowed due to the nature of the terrain.

Early research work with experimental results for landing maneuvers considered horizontal flat and stable landing surfaces. To land, the aircraft was simply commanded through position or velocity tracking maneuvers until contact with the ground occurred (see [11], [12]). The more challenging problem of landing an autonomous helicopter on an oscillating platform, such as the deck of a ship at sea, was considered in [13], and more recently, a landing controller able to cope with a landing platform that is vertically moving with unknown dynamics developed in [14], where landing is achieved based on optical flow measurements. The related problem of landing on a horizontally moving platform was studied in [15], where the authors tackle the problem of landing the vehicle on a platform moving in the horizontal plane. The quadrotor control system is decomposed in an outer loop for translational velocity control and an inner loop for attitude control, so as to decouple both dynamics. The controller, however, assumes perfect-state measurement and tracking, with no emphasis given to robustness.

Recently, particular emphasis has been laid on other flight conditions where interaction with the environment also occurs. In [16] and [17], solutions for landing aerial vehicles by perching on vertical walls are studied and an armlike extension to interact with objects [18] has also been proposed. These flight regimes are considerably more challenging for the aircraft operation than FF as even small errors can result in catastrophic consequences, due to the proximity between the rotor's fast rotating blades to the environment. In addition, special attention has to be paid to the dynamics of the vehicle, as these change according to the type of contact being established. As such, for a successful operation in a wide range of mission scenarios, robust controllers must be designed for each flight regime that ensures that the vehicle completes the maneuver without incidents, despite possible parameter or modeling uncertainties. Further exploration of flight modes where physical contact with the environment occurs culminated in [19], which focuses on the interaction of a ducted-fan aerial vehicle with a vertical surface, where sliding is allowed, which can be regarded as parallel to the proposed quadrotor maneuver of sliding on the ground. The ducted-fan is a VTOL rotorcraft vehicle able to hover like a helicopter or quadrotor but whose fuselage is more appropriate for general contact with the environment, as the sole rotating propeller is protected from accidental contacts by the duct.

The essence of the different dynamic behaviors of an aerial vehicle when interacting with the environment and the conditions for commutation between each operating mode can be easily captured by a hybrid automaton. Hybrid automata constitute a subset of the larger class of hybrid dynamical systems [20] and allow the modeling of a complex system in a modular way by collecting simpler dynamical models, each one focusing only on a precise operating mode of the system. Hybrid controllers have been successfully applied to trajectory tracking of aerial vehicles in different setups, from which we highlight two. In [21], a hybrid controller is designed to fulfill multiple hierarchical objectives and includes a tactical planner, responsible for the higher level behavior of the aircraft, and a trajectory planner, which generates the desired trajectory for each mode. A different hierarchical control architecture for aggressive maneuvering applicable to autonomous helicopters is proposed in [22], wherein the hybrid controller is based on an automaton whose states represent feasible trajectory primitives. In both papers, different states of the automata correspond to different trajectories and not to different dynamics of the vehicle. In addition, in the former work, the overall switched system stability analysis is not presented and, in the latter, perfect tracking of the nominal trajectories is assumed.

In [23], guarantees on the safety and performance of hybrid automata modeling robotic aerial vehicles are achieved through reachability analysis using a dynamic game formulation with Hamilton–Jacobi methods under some appropriate assumptions about the control and disturbance. Experimental results are presented for a quadrotor performing a backflip maneuver divided into sections, each corresponding to a different operating mode. Starting from the desired final location, backward reachable sets (sets from which the desired state can be provably attained) are derived for the vehicle through optimization techniques, leading to a final feasible maneuver. However, the vehicle dynamics do not change during the maneuver, unlike the proposed landing maneuver where a collision with the ground leads to a jump in the system state and changes the vehicle dynamics.

In this paper, we build on the works presented in [24] and [25] and propose a hybrid flight controller that ensures a successful completion of a landing maneuver, from a FF configuration to a complete halt, for a quadrotor vehicle in challenging circumstances. In the spirit of [24], a hybrid automaton is used to model the vehicle, thereby encapsulating the complete dynamics of the different flight regimes that the vehicle must traverse. Once the hybrid automaton is defined, the landing problem is addressed as a combination of trajectory generation and trajectory tracking control problems. In particular, both the reference signals and the feedback laws for each operating mode are derived considering explicitly the presence of uncertainties. The references are designed such that their practical, and not perfect, tracking ensures that the desired transitions happen, despite the possible presence of uncertainties. The idea of concatenating maneuvers for which a successful transition can be proven to happen has some similarities with the reachable sets idea in [23], leading to the same end result (a provable complete maneuver) albeit through different intermediate concepts—concatenation of transition maneuvers versus reachable sets for the desired final location.

The control methodology presented in the sequel requires that the current operative mode of the UAV is known. For the specific landing operation, the operative mode can be retrieved by merging the information derived from contact or force sensors, to be placed at each extremity of the vehicle's landing gear, with the knowledge of the velocity and the attitude of the vehicle obtained through a standard inertial navigation unit. If the position of the landing slope is known, the operating state can even be inferred from just the position, attitude,

and velocity of the vehicle, without resorting to additional sensors.

The main contribution of this paper consists of the explicit design of the hybrid automaton model, robust reference maneuvers, and low-level controllers for the robust landing of a quadrotor vehicle and consequent experimental evaluation of the proposed architecture. We present the dynamics for a quadrotor pivoting and/or sliding along a slope and construct a robust hybrid controller, along with appropriate reference trajectories, that allows for fully autonomous robust landing of the vehicle. The performance and robustness characteristics of the proposed hybrid controller guarantee that the vehicle does not overturn and that the landing impact is sufficiently smooth so that the vehicle does not rock. The proposed landing procedure is tested in an experimental setting using off-the-shelf quadrotors and a motion capture system is used that allows for state feedback. A preliminary version of this paper can be found in [26].

The remainder of this paper is organized as follows. Section II presents the hybrid automaton model for the vehicle. The robust control architecture is discussed in Section III, which entails the generation of the robust reference maneuvers, low-level controllers, and the supervisor. The experimental setup used to test the control algorithms is detailed in Section IV, and Section V presents the experimental results. Finally, the concluding remarks and future work considerations are presented in Section VI.

II. Quadrotor Hybrid Model

The UAV considered in this paper is a quadrotor aircraft actuated in force, generated by the four propellers, with VTOL capabilities. For the sake of simplicity, we consider only the planar dynamics on the configuration manifold $\mathrm{SE}(2) = \mathbb{S}^1 \times \mathbb{R}^2$. A 2-D landing corresponds to the physical quadrotor having two contact points with the ground, restraining it to slide over the 2-D plane and to rotate around the axis defined by the two contact points. Were the quadrotor to be allowed to have only one contact point it could pivot around it with 2 DOF, rendering the general 3-D control problem more complex and with no added value. Let $\mathbf{n}$ be the normal vector to the 3-D landing slope and $\mathbf{g}$ be the vector aligned with gravity direction. The vector $\mathbf{n}$ must be constant for the section of the landing slope needed for landing, depending on the size of the quadrotor and the desired sliding trajectory. This last requirement of continuity results in a landing plane that is vertical so that the contact of the left and right landing gears occurs simultaneously, and the quadrotor does not pivot around a single contact point. Although the proposed hybrid controller framework can be extended to three dimensions using the same mathematical modeling principles, the authors feel it would not bring added benefits.

Fig. 1(a) presents a graphical description of the quadrotor geometry and the landing environment. The ground is modeled as a flat surface at an angle β with the horizontal. A body-fixed frame $\{\mathcal{B}\} = \{\mathrm{CM}, \vec{i}_B, \vec{k}_B\}$ is attached to the quadrotor's center of mass (CM), with the vector $\vec{k}_B$ pointing upward, along the thrust direction. The inertial frame $\{\mathcal{I}\} = \{O, \vec{i}, \vec{k}\}$ is defined

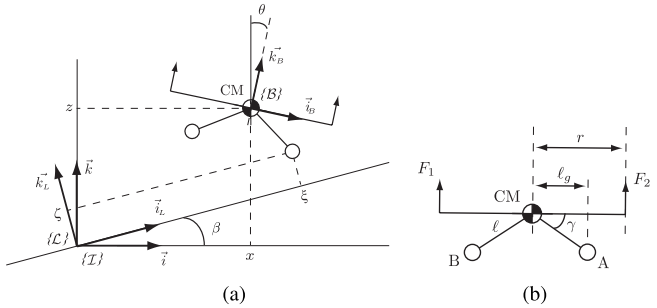

Fig. 1. Takeoff slope and quadrotor. (a) Reference frames. (b) Quadrotor geometry.

by the vectors $\vec{i}$ and $\vec{k}$ that point north and up, respectively. An additional frame $\{\mathcal{L}\} = \{O, \vec{i}_L, \vec{k}_L\}$, denoted by *slope frame*, is attached to the origin of $\{\mathcal{I}\}$ and rotated with respect to $\{\mathcal{I}\}$ by an angle β. The angle θ denotes the rotation angle from the inertial frame to the body frame. The planar model of the quadrotor shown in Fig. 1(b) has two counter-rotating motors for propulsion, generating the aerodynamic forces F_1 and F_2, and a landing gear with two points of contact with the ground, denoted by A and B. The distance from the CM to each motor and to each contact point are denoted by r and ℓ, respectively. The angle with vertex in CM and subtended by the motor and contact point is denoted by γ. The shorthand $\ell_g = \ell \cos(\gamma)$ is introduced to simplify mathematical expressions.

To simplify the description of the various quadrotor dynamics, the state of the quadrotor is expressed in different coordinate systems, according to its operative mode. When in FF, the quadrotor state is described by the tuple (x, z, θ) and its derivative, where x, z are the CM coordinates in the inertial frame θ is the quadrotor tilt angle. In situations where contact with the ground occurs, the quadrotor state is described by the tuple (ξ, ζ, θ) and its derivative, wherein ξ, ζ are the coordinates of point A in the slope frame and θ is the quadrotor tilt angle. This change of coordinates given by

$$\begin{aligned} \xi &= x\cos\beta + z\sin\beta + \ell\cos(\theta + \gamma + \beta) \\ \zeta &= -x\sin\beta + z\cos\beta - \ell\sin(\theta + \gamma + \beta) \end{aligned}$$

helps to decouple the translational motion of the contact point along the slope, captured by ξ, from the rotational motion of the quadrotor around the contact point, embedded in θ. A depiction of the inertial and the slope frames is presented in Fig. 1(a), together with a representation of the vehicle location in each frame.

For the development of the quadrotor hybrid automaton, we consider five operating modes, corresponding each mode to the different dynamics that the vehicle is subject to. The modes are distinguished by the number of contact points of the landing gear with the ground and the existence of relative movement between the contact point and the ground. The operating modes are defined as follows.

1) *FF:* In this operating mode, the quadrotor is in FF and no contact with the landing slope occurs.
2) *Takeoff and Landing (TL and TLs):* In a *takeoff-and-landing* situation, there exists a single contact point between the quadrotor and the ground, shown as A

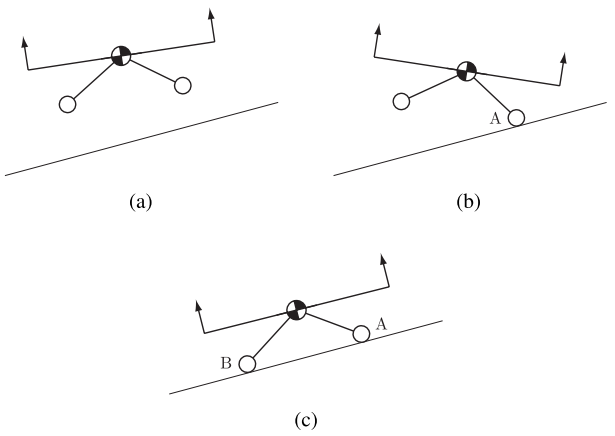

Fig. 2. Quadrotor operating modes. (a) FF. (b) Takeoff-and-landing and takeoff-and-landing sliding (TL/TLs). (c) Landed and landed sliding (LL/LLs).

in Fig. 2(b). The shorthand notation TL denotes the nonsliding situation and TLs the takeoff-and-landing mode where sliding exists between the quadrotor and the ground. In this paper, we focus on landings where point A hits the ground first and acts as pivot, since it leads to more natural landing maneuvers. Landing situations where B is the first point of impact with the landings slope are dealt analogously within the proposed framework as they correspond to considering a landing with point A as pivot where the slope angle β is negative.

3) *Landed (LL and LLs):* In the *landed* operating mode, the landing gear is in full contact with the ground, with both points A and B touching the landing slope, as observed in Fig. 2(c). The shorthand notation LL denotes the nonsliding situation and LLs the landing operative mode where the quadrotor slides on the ground.

The quadrotor presents different dynamics in each operating mode. These were derived in [25] and are presented in the discussion of the hybrid automata model for completion. In determining the discrete jumps between operating states during the landing maneuver, we assume that the collisions are inelastic.

A. Hybrid Model of the Overall Dynamics

A description of the overall quadrotor dynamics is obtained by means of a hybrid automaton whose states correspond to the operating modes described above. A hybrid automaton is identified by the following objects, instanced here for the specific case of the planar quadrotor.

1) Operating Modes: The quadrotor automaton comprises the set $\mathcal{Q}$ of *operating modes*, denoted by $\mathcal{Q} = \{\text{LL, LLs, TL, TLs, FF}\}$, with the meaning *landed*, *landed sliding*, *takeoff and landing*, *takeoff and landing sliding*, and FF, respectively.

2) Domain Map: The state of the system $\mathbf{x} \in \mathbb{R}^6$ is described by either $(x, \dot{x}, z, \dot{z}, \theta, \dot{\theta})$ or $(\xi, \dot{\xi}, \zeta, \dot{\zeta}, \theta, \dot{\theta})$. When the UAV is in contact with the ground (LL, LLs, TL, and TLs operating modes), the preferred reference frame and the state $\mathbf{x} = (x, \dot{x}, z, \dot{z}, \theta, \dot{\theta})$ are the $\{\mathcal{L}\}$ frame, yielding $\mathbf{x} = (\xi, \dot{\xi}, \zeta, \dot{\zeta}, \theta, \dot{\theta})$, while the $\{\mathcal{I}\}$ frame is preferred for the FF mode. The inputs F_1 and F_2, which correspond to the forces generated by the propellers, are bounded by a minimum and maximum value, leading to the definition of the input domain $U \subset \mathbb{R}^2$ as the compact interval $U = [F_{\min}, F_{\max}] \times [F_{\min}, F_{\max}]$. The domain mapping $\mathcal{D} : \mathcal{Q} \rightrightarrows \mathbb{R}^6 \times \mathbb{R}^2$ defines, for each operating mode, the set of values that the state $\mathbf{x}$ and the control input u may take.

3) Flow Map: The flow map $f : \mathcal{Q} \times \mathbb{R}^6 \times \mathbb{R}^2 \to \mathbb{R}^6$ describes for each operating mode $q \in \mathcal{Q}$ the evolution of the state variables. In each operating mode q, we have the dynamic system $\dot{\mathbf{x}} = f(q, \mathbf{x}, u)$, where each function $f(q, \mathbf{x}, u)$ is derived from the differential equations that govern the movement of the quadrotor vehicle, which we detail now.

a) Free flight: In this operating mode, the aircraft is airborne. The FF planar quadrotor is modeled as a rigid body evolving on $\mathrm{SE}(2) = \mathbb{S}^1 \times \mathbb{R}^2$, subject only to the aerodynamic forces generated by the motors and propellers. This leads to the quadrotor dynamics

$$m\ddot{x} = (F_1 + F_2)\sin\theta + \delta_x \tag{1a}$$

$$m\ddot{z} = (F_1 + F_2)\cos\theta - mg + \delta_z \tag{1b}$$

$$J\ddot{\theta} = (F_1 - F_2)r \tag{1c}$$

where m and J denote, respectively, the mass and moment of inertia of the vehicle, g the gravity acceleration, and δ_x and δ_z the exogenous disturbances acting along the lateral and vertical directions, respectively. Disturbances in the angle dynamics fit within the proposed model but are not considered because they are, in general, negligible. To support the use of a simplified dynamical model, such as the one described above, the FF controller is designed to be robust to external disturbances, which can encompass wind disturbances and modeling uncertainties, up to a given limit.

b) Partial interaction with the ground: In the TL and TLs modes of operation, there is only one contact point of the quadrotor with the ground, as evidenced in Fig. 2(b). The vehicle's motion is restricted to a rotation around the contact point A and translation of the contact point along the slope. The friction coefficient μ between the landing gear and the glide slope materials influences these dynamics, and we assume that the static and dynamic coefficients are equal. In general, only a rough estimate of the friction coefficient is known and, as such, the controller are nominally designed for $\mu = \mu_0$ but are ϵ-robust for a range of μ values. The slope is assumed to be sufficiently smooth and cleared of obstacles so that the quadrotor is able to slide without getting stuck. The roughness that can be allowed on the terrain depends on the terminations of quadrotor's landing gear. Designing the contact points with smooth spherical endings reduces the cases where the vehicle can be stuck due to terrain roughness.

The dynamics in this operating mode are obtained from the Euler–Lagrange equations for the quadrotor system where the Lagrangian is

$$\mathcal{L} = \frac{1}{2}m(\dot{x}^2 + \dot{z}^2) - mgl\sin(\theta + \gamma).$$

Using the virtual forces F_ξ and F_θ described in the sequel, the resulting dynamics are given by

$$\ddot{\xi} = F_\xi + h_\xi(\theta, \dot{\theta}, \dot{\xi}, \mu) \tag{2a}$$

$$\ddot{\theta} = F_\theta + h_\theta(\theta, \dot{\theta}, \dot{\xi}, \mu) \tag{2b}$$

where

$$\begin{aligned} &h_\xi(\theta, \dot{\theta}, \dot{\xi}, \mu) \\ &= \frac{1}{J + m\ell^2 \cos^2(\beta + \gamma + \theta)} \\ &\quad \times (-g(J + m\ell^2) \cdot (\mu \cos\beta \operatorname{sign}(\dot{\xi}) + \sin\beta) \\ &\qquad + gm\ell^2 \cos(\gamma + \theta) \sin(\gamma + \theta + \beta) \\ &\qquad - \ell(J + m\ell^2) \cos(\gamma + \theta + \beta)\dot{\theta}^2) \\ &h_\theta(\theta, \dot{\theta}, \dot{\xi}, \mu) \\ &= \frac{m\ell}{J + m\ell^2 \cos^2(\beta + \gamma + \theta)} \\ &\quad \times (\cos(\gamma + \theta + \beta) \cdot (-g \cos\beta + \ell \sin(\gamma + \theta + \beta)\dot{\theta}^2) \\ &\qquad + g\mu \cos\beta \sin(\gamma + \theta + \beta) \operatorname{sign}(\dot{\xi})). \end{aligned}$$

The virtual inputs F_θ and F_ξ are directly related to the real quadrotor inputs F_1 and F_2 through

$$\begin{pmatrix} F_\xi \\ F_\theta \end{pmatrix} = L(\theta)^{-1} G(\theta) M \begin{pmatrix} F_1 \\ F_2 \end{pmatrix} \tag{3}$$

where the matrices M, $G(\theta)$, and $L(\theta)$ are given by

$$\begin{aligned} M &= \begin{pmatrix} 1 & 1 \\ r + \ell_g & \ell_g - r \end{pmatrix} \\ G(\theta) &= \begin{pmatrix} \sin(\theta + \beta) + \mu \operatorname{sign}(\dot{\xi}) \cos(\theta + \beta) & 0 \\ 0 & 1 \end{pmatrix} \\ L(\theta) &= m \begin{pmatrix} 1 & \ell \sin(\theta + \gamma + \beta) \\ \ell \sin(\theta + \gamma + \beta) & \ell^2 + J/m \end{pmatrix} \end{aligned} \tag{4}$$

respectively. This input transformation is always well defined, since $L(\theta)$ is invertible, independently of the tilt angle. The dynamics (2) apply only to a quadrotor *sliding* along the slope. In the *takeoff-and-landing* operating mode, where the contact point A is fixed, the ξ position is constant and the dynamic system is reduced to (2b) with $\dot{\xi} = 0$, resulting in

$$\ddot{\xi} = 0 \tag{5a}$$

$$\ddot{\theta} = F_\theta + h_\theta(\theta, \dot{\theta}, 0, \mu). \tag{5b}$$

Equations (2) and (5) describe a four-state dynamical model for the vehicle. The coordinates of the CM and its derivatives are uniquely defined by the states ξ, $\dot{\xi}$, θ, and $\dot{\theta}$.

c) Complete interaction with the ground: In the LL and LLs operating modes, the vehicle is completely landed and only the gravity and the ground contact friction affect the motion of the vehicle. The dynamic model for the LLs operating mode is completely described by the dynamical system

$$m\ddot{\xi} = -mg \sin\beta - \mu \operatorname{sign}(\dot{\xi}) F_N \tag{6a}$$

$$\dot{\theta} = 0 \tag{6b}$$

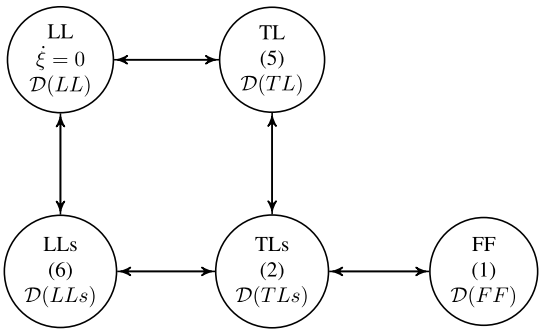

Fig. 3. Planar quadrotor hybrid automaton.

with reaction force F_N given by

$$F_N = (mg \cos\beta - (F_1 + F_2) \cos(\theta + \beta)).$$

When in the LL operating mode, because the collisions are inelastic and the quadrotor does not rock, this reduces to

$$\dot{\xi} = 0$$
$$\dot{\theta} = 0$$

and the vehicle's state remains unchanged.

4) Edges: The set of edges $\mathcal{E} \subset \mathcal{Q} \times \mathcal{Q}$ includes all the pairs (q_1, q_2) such that a transition between the modes q_1 and q_2 is possible, for some combinations of state and actuation. For the takeoff and landing procedures, we consider the transitions shown in Fig. 3. Direct edges linking LL to FF or FF to LL are not modeled as these suffer from robustness issues and are not used for the maneuvers. Nonetheless, these transitions can be equivalently obtained by considering sequential instantaneous transitions through the intermediate operative modes TL and TLs.

5) Guard Mapping: The set-valued guard mapping $\mathcal{G} : \mathcal{E} \rightrightarrows \mathbb{R}^6 \times \mathbb{R}^2$ determines, for each edge $(q_1, q_2) \in \mathcal{E}$, the set $\mathcal{G}(\{q_1, q_2\})$ to which the quadrotor state $\mathbf{x}$ and inputs F_1, F_2 must belong so that a transition from q_1 to q_2 can occur. There are three main groups of transitions to consider for the landing procedure. First, the operating mode transitions between FF and the TLs operating mode depend on the force perpendicular to the slope $F_\perp$

$$F_\perp(\theta, F_1, F_2) = (F_1 + F_2) \cos(\theta + \beta) - mg \cos\beta$$

and the height of the quadrotor relative to the ground. The dependence gives rise to the guard sets

$$\mathcal{G}(\{\text{FF}, \text{TLs}\}) = \{(\mathbf{x}, u) \in \mathcal{D}(\text{FF}) : \zeta \leq 0 \wedge F_\perp(\theta, F_1, F_2) < 0\}$$

$$\mathcal{G}(\{\text{TLs}, \text{FF}\}) = \{(\mathbf{x}, u) \in \mathcal{D}(\text{TLs}) : F_\perp(\theta, F_1, F_2) \geq 0\}$$

where $\wedge$ denotes the logical AND operator. Second, the transitions where the quadrotor goes from a state with one contact point (TL and TLs operating modes) to two contact points (LL and LLs) are governed by the sign of the torque F_τ at point A

$$F_\tau(\theta, F_1, F_2) = (F_1 + F_2) l_g + (F_1 - F_2) r - mg\ell \cos(\theta + \gamma)$$

and by the angle of the vehicle with the slope, $\theta + \beta$. The inverse transition depends only on the sign of F_τ.

The corresponding guard sets are defined as

$$\mathcal{G}(\{\text{TL}, \text{LL}\}) = \{(\mathbf{x}, u) \in \mathcal{D}(\text{TL}) : \theta + \beta \leq 0 \wedge F_\tau(\theta, F_1, F_2) < 0\}$$
$$\mathcal{G}(\{\text{LL}, \text{TL}\}) = \{(\mathbf{x}, u) \in \mathcal{D}(\text{LL}) : F_\tau(-\beta, F_1, F_2) \geq 0 \vee \theta > -\beta\}$$

with analogous versions for the situation where sliding occurs. Finally, we have the transitions between the *at rest* and the *sliding* modes, which are governed by the relation between the force along the slope at the contact point ($F_\xi + h_\xi$) and the perpendicular force $F_\perp$, encapsulated in the function

$$F_{\text{slide}}(\theta, \dot{\theta}, F_1, F_2, \mu) = |F_\xi(\theta, \dot{\theta}, \mu, F_1, F_2) + h_\xi(\theta, \dot{\theta}, 0, \mu)| - \mu \frac{mg\cos\beta}{m\cos^2(\theta+\beta+\gamma)} + \mu \frac{(F_1+F_2)\cos(\theta+\beta)}{m\cos^2(\theta+\beta+\gamma)}.$$

The contact is modeled according to the Coulomb friction model and a transition from a nonsliding mode to a *sliding* mode occurs for $F_{\text{slide}} > 0$, whereas a reverse transition happens when the velocity of the contact point along the slope reaches zero and $F_{\text{slide}} < 0$. Expressed mathematically, one gets

$$\mathcal{G}(\{\text{TLs}, \text{TL}\}) = \{(\mathbf{x}, u) \in \mathcal{D}(\text{TLs}) : \dot{\xi} = 0,\ F_{\text{slide}}(\theta, \dot{\theta}, F_1, F_2, \mu) \leq 0)\}$$
$$\mathcal{G}(\{\text{TL}, \text{TLs}\}) = \{(\mathbf{x}, u) \in \mathcal{D}(\text{TL}) : F_{\text{slide}}(\theta, \dot{\theta}, F_1, F_2, \mu) > 0)\}$$

and analogous expressions for the guard sets between the LL and LLs transitions. In the landed operating mode, the function regulating slide transitions is reduced to

$$F_{\text{slide}}(-\beta, 0, F_1, F_2, \mu) = mg\sin\beta - \mu(mg\cos\beta - (F_1+F_2)).$$

6) Reset Maps: For each $(q_1, q_2) \in \mathcal{E}$ and $(\mathbf{x}, u) \in \mathcal{G}(\{q_1, q_2\})$, the reset map $\mathcal{R} : \mathcal{E} \times \mathbb{R}^6 \times \mathbb{R}^2 \to \mathbb{R}^6$ identifies the jump of the state variable $\mathbf{x}$ during the operating mode transition from q_1 to q_2. The jumps in the state reflect instantaneous changes that are caused by the collisions of the contact points with the landing slope and also the use of either frame $\{\mathcal{L}\}$ or $\{\mathcal{I}\}$ to describe the state, according to the operating mode.

The only reset maps that result from physical interaction are the ones governing the transitions from FF to TLs and TL to LL. In particular, for reference trajectory generation, we model the map $\mathcal{R}(\{\text{TL}, \text{LL}\}, (\mathbf{x}, u))$ under the assumption of an inelastic collision and the map $\mathcal{R}(\{\text{FF}, \text{TLs}\}, (\mathbf{x}, u))$ is modeled under the assumption of inelastic impact along the perpendicular of the landing slope and by considering energy conservation (see [10, Ch. 6.2.1] among others). This results in a trivial transition from TL to LL where the angular velocity of the vehicle is simply set to zero when the second landing gear makes contact with the landing slope. The transition from FF to the TLs operating mode is more complex and is analyzed in the sequel. The kinetic energies of the vehicle ignoring the constant lateral velocity along the slope before and after the impact is given, respectively, by

$$E^- = \frac{1}{2}m\left(\dot{\zeta}_{\text{CM}}^-\right)^2 + \frac{1}{2}m\left(\dot{\xi}_{\text{CM}}^-\right)^2 + \frac{1}{2}\mathbb{J}(\dot{\theta}^-)^2$$

and

$$E^+ = \frac{1}{2}m\left(\dot{\xi}_{\text{CM}}^+\right)^2 + \frac{1}{2}m\ell^2(\theta^+)^2$$

where $(\xi_{\text{CM}}, \zeta_{\text{CM}})$ are the coordinates of the CM in frame $\{\mathcal{L}\}$. With $c_E \in (0, 1]$ an energy loss coefficient, it turns out that $(E^+) = c_E(E^-)$ and then

$$\dot{\theta}^+ = \sqrt{c_E}\sqrt{\left(\dot{\zeta}_{\text{CM}}^-/(\ell^2)\right)^2 + (J(\dot{\theta}^-)/(m\ell^2))^2}$$

and

$$\left(\dot{\xi}_{\text{CM}}^+\right) = \sqrt{c_E}\left(\dot{\xi}_{\text{CM}}^-\right).$$

Then by considering the constraint on ζ_{CM} characterizing $\mathcal{D}_{\text{TLs}}$ and $\mathcal{D}_{\text{TLs}}$, we obtain $\dot{\zeta}_{\text{CM}}^+ = \dot{\theta}^+\ell\cos(\theta^- + \gamma + \beta)$.

III. Robust Control Strategy and Architecture

With the hybrid automaton defined, the problem of performing a landing maneuver can be reformulated as a problem of changing the operative mode q from the initial FF mode FF to the final landed configuration LL, by going through the intermediate states. The control strategy must achieve the transition between the desired operating modes with robustness to uncertainties in the model and the environment all the while avoiding transitions to undesired modes. The sequence of operating modes for the landing maneuver is chosen as FF, TLs, TL, and finally LL, for which the transitions can be achieved robustly. As a remark, we note that sliding is not mandatory in the proposed framework. It can be avoided by considering an instantaneous transition from TLs to the TL state, resulting in a more traditional landing maneuver while maintaining the robustness and performance guarantees.

Following the general framework proposed in [24], the control problem is divided into two different steps. The first step amounts to computing, for each of the three desired transitions (FF $\to$ TLs, TLs $\to$ TL, and TL $\to$ LL), reference trajectories for both the states $\mathbf{x}$ and the inputs u of the system, jointly denoted by the *reference maneuvers*. For each operating mode $q \in \mathcal{Q}$, the reference maneuvers are designed to guarantee robustness with respect to a design parameter $\epsilon > 0$, meaning that practical tracking of the reference trajectories, up to a tracking error ϵ (in both state and input), ensures that only the desired transition is achieved. The second step consists of designing feedback control laws for each operating mode guaranteeing that for the proposed reference maneuvers and despite parametric uncertainties and exogenous disturbances, the tracking error (both in the state and in the input) is upper bounded by the design parameter ϵ so that the planned transition is enforced. The parameter ϵ provides robustness to the landing maneuver. It can be chosen so that the quadrotor is guaranteed not to overturn during the maneuver and so that dangerous angles are not reached during the landing and sliding procedure.

The control architecture (sketched in Fig. 4) comprises a set of low level controllers, associated with the specific operative modes in which the vehicle operates, and a supervisor. The latter, through sensor readings, detects the current operating mode of the quadrotor and selects the appropriate low-level feedback controller to be used. This ensures that for each

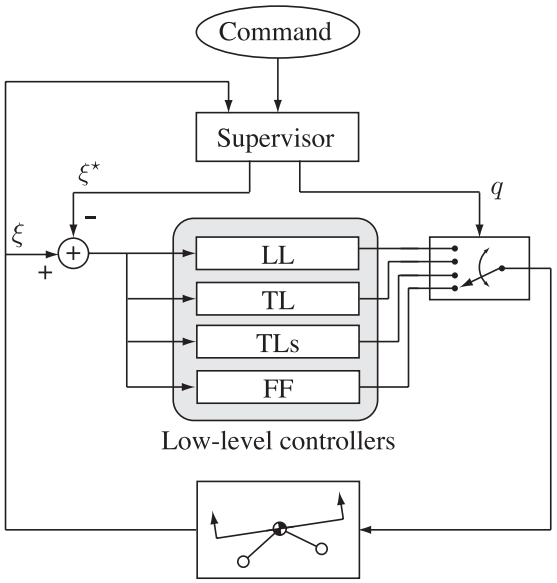

Fig. 4. Proposed control architecture, featuring the supervisor, and low-level controllers.

operating mode, the tracking errors are always within the allowable bound for the robust transition maneuver to occur. As required by the hybrid control framework, the robustness is quantified in terms of the design parameter $\epsilon > 0$ that roughly expresses how far the actual motion of the system's state and input can be with respect to the reference maneuver to have the desired transition effectively imposed.

Stability of the proposed landing maneuver and hybrid controller is ensured by adopting the framework in [24]. By following the framework requirements and always staying ϵ-far from undesired transitions, we ensure that desired transitions are eventually attained. The local controllers also guarantee that chattering does not occur since transitioning back to the previous operating mode is an undesired transition.

A. Robust Reference Maneuvers

To precisely define the maneuvers of interest, we denote by $\upsilon_q(t) = (\xi(t), u(t))$ a maneuver taking place in the operating mode $q \in \mathcal{Q}$ and by $\mathrm{gr}\,\upsilon_q$ the graph of the maneuver in a certain time interval. According to [24], toward which the reader is referred for further mathematical details, three different types of maneuvers are defined. The first one, which is denoted by *ϵ-robust q_1-single maneuver in* $[t_0, t_1)$, is such that the state and the input do not intersect any guard condition to maintain the same single operating mode q_1. The second type, denoted by *ϵ-robust $q_1 \to q_2$ approach maneuver in* $[t_0, T]$, is such that at time T, the maneuver robustly belongs to the desired guard set, $\mathcal{G}(\{q_1, q_2\})$, to switch to the operating mode q_2. The last one, the *$q_1 \to q_2$ transition maneuver in* $[t_0, t_1)$, is obtained as a combination of an ϵ-robust $q_1 \to q_2$ approach maneuver and a set of ϵ-robust q_2-single maneuvers. We now present multiple straightforward robust approach trajectories whose practical tracking leads the quadrotor from FF to a final landed position in a controlled manner. The maneuvers are parameterized by their starting conditions and are combined to generate the robust transition maneuvers.

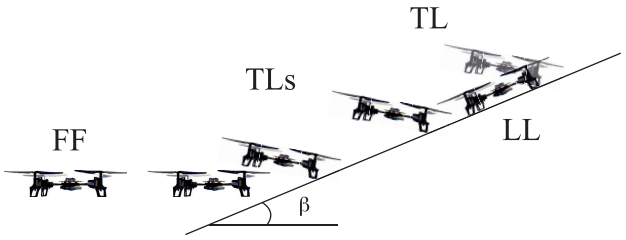

Fig. 5. Sketch of a complete quadrotor landing maneuver.

The proposed complete landing maneuver is shown in Fig. 5. The landing procedure starts in FF, where a horizontal landing path is tracked. This eventually leads to a collision with the sloped ground, at which instant the supervisor selects the TLs controller and starts tracking a reference maneuver that leads the quadrotor to the TL state. The quadrotor then slides up the slope, tracking a TLs to TL trajectory, until it comes to a halt at a desired location. Upon coming to a halt, the quadrotor transitions to the TL operating mode and the supervisor uses the TL low-level controller to track a TL to LL trajectory that finally levels the quadrotor with the ground, without starting to slide again. Once all the landing gear contact points touch the ground and the final transition to the landed mode is complete, the motors are turned OFF and the quadrotor remains at rest.

For the proposed maneuvers, it must be verified that the undesired transitions are indeed avoided with the proposed controllers, for all the possible disturbances. For complex dynamics, guard sets, and disturbances, this exhaustive search for a trajectory can be performed with optimization techniques, such as the ones proposed in [25], wherein obstacle avoidance and other additional constraints can also be integrated.

1) FF $\to$ TLs Robust Transition Maneuver: For taking the aircraft from FF to the takeoff-and-landing sliding operating mode, we propose a maneuver that leads to the quadrotor sliding up. In that situation, we have $\dot{\xi} > 0$, which results in a G matrix that is well conditioned [see (4)], thereby avoiding problems when inverting (3) to obtain the inputs F_1 and F_2. In addition, the maneuver was chosen to have a minimal impact on the quadrotor upon touchdown on the landing slope. The quadrotor is chosen to track a horizontal line at a constant velocity until the contact point A of the landing gear touches the landing slope. For the quadrotor model in (1), the reference maneuver is defined as

$$\begin{aligned} x^\star(t) &= x_0 + \upsilon_x(t - t_0) \\ z^\star(t) &= z_0 \\ \theta^\star(t) &= 0 \\ F_1^\star(t) = F_2^\star(t) &= mg/2 \end{aligned}$$

for the positive lateral velocity υ_x, initial conditions x_0, $z_0 \in \mathbb{R}$, and initial time $t_0 \in \mathbb{R}$. The positive velocity corresponds to a landing maneuver where the quadrotor lands from the lower side of the slope. If tracked with an error smaller than ϵ, this maneuver ensures that only one of the quadrotor's landing gears hits the slope and that the quadrotor starts to

Fig. 6. Quadrotor performing a TLs to TL robust transition maneuver.

slide on the ground, forcing a transition to the TLs mode. The time instant at which the transition occurs depends on the location of the slope, the quadrotor initial position (x_0, z_0), and the lateral approach velocity v_x.

2) TLs → TL Robust Transition Maneuver: Following Fig. 5, in the TLs operating mode, the quadrotor tracks a straight line along the slope and decreases its velocity, until it comes to a halt. We define a reference maneuver with constant acceleration for the contact point and a fixed tilt angle as follows:

$$\xi^\star(t) = \xi_0 + v_\xi(t - t_0) - a_\xi(t - t_0)^2$$
$$\theta^\star(t) = \theta_0$$

for the initial conditions $\xi_0 \in \mathbb{R}$ and positive parameters v_ξ, a_ξ, and θ_0. The corresponding reference inputs $F_1^\star(t)$ and $F_2^\star(t)$ are obtained by dynamic inversion of vehicle model. A set of maneuvers with different initial condition parameters at the initial time instant t_0 is considered so as to cover the whole region of possible initial conditions that arises when the tracking of the preceding maneuver is not perfect. The tilt angle θ_0 that the quadrotor follows while sliding should be slightly positive so that the quadrotor is able to slide along the slope robustly, without returning to the FF operating mode, as depicted in Fig. 6. The transition to TL occurs when $\dot{\xi} = 0$. That final time instant, denoted by t_f, depends on the initial velocity v_ξ and the desired acceleration a_ξ. The final landing location along the slope also depends on these two parameters and the initial location of the quadrotor. It can be made constant for all trajectories by varying the acceleration parameter a_ξ

$$a_\xi = \frac{v_\xi^2}{\xi^\star(t_f) - \xi^\star(t_0)}.$$

3) TL → LL Robust Transition Maneuver: Once the quadrotor comes to a halt, the objective is to bring it to the slope level, without inducing a sliding movement again. In this operating mode, we are only interested in controlling the tilt angle, for which we define the reference trajectory

$$\theta^\star(t) = \theta_0 - v_\theta t \tag{7}$$

for a positive parameter v_θ. The quadrotor is finally leveled with the landing slope when $\theta^\star(t) = -\beta$. The reference input is determined by (7) and the reference *total thrust*, $T^\star(t) = F_1^\star(t) + F_2^\star(t)$, which is chosen to converge from its initial value down to zero. In order for the maneuver to be robust, the balance between $T^\star(t)$ and $\theta^\star(t)$ must be such that the vehicle is always ϵ far from restarting to slide during the whole transition maneuver. For the duration of this transition maneuver, the displacement of the landing gear contact point is constant, i.e. $\xi(t) = \xi_0$.

B. Single Operating Mode Controllers

In this section, we detail the controllers that are employed in each operating mode to drive the vehicle along the desired transition trajectories, to achieve a successful landing maneuver. These are based on [25] and [26], where locally input-to-state-stable (locally-ISS) controllers for FF and for the operating states where contact occurs have been developed. In a locally ISS system (see [27]), the external disturbances have a bounded effect on the state, which depends on the magnitude of the disturbances. Each of the controllers is required to stabilize the closed-loop system, for the appropriate dynamics, in a practical sense. Hence, despite possible disturbances and perturbations, the tracking error remains within ϵ bounds and an operating mode transition is guaranteed to occur.

1) Free Flight Controller: To steer the vehicle in FF, we use the backstepping controller developed in [25], restricted to a 2-D setup. The state feedback controller imbues the error system with a Lyapunov function with strictly negative derivative, resulting in a closed-loop system that is locally ISS with respect to the external disturbances considered in (1). Given a disturbance bound, the control gains can be tuned so as to render the closed-loop error bound sufficiently small. As a consequence, the resulting closed-loop error can always be bounded by ϵ.

2) Takeoff-and-Landing Sliding Controller: With $u^\star(t) = (F_1^\star(t), F_2^\star(t)) : [t_0, t_f] \to \mathbb{R}^2$ and $\xi^\star(t) = (\xi^\star(t), \dot{\xi}^\star(t), \theta^\star(t), \dot{\theta}^\star(t)) : [t_0, t_f] \to \mathbb{R}^4$, a robust reference TLs to TL maneuver, we define [see (3)]

$$\begin{pmatrix} F_\xi^\star(t) \\ F_\theta^\star(t) \end{pmatrix} = L(\theta^\star(t))^{-1} G(\theta^\star(t)) M \begin{pmatrix} F_1^\star(t) \\ F_2^\star(t) \end{pmatrix}$$

for all $t \in [t_0, t_f]$. The control law for the TLs dynamics (2) is then chosen as

$$F_\xi(t) = -K_P(\xi - \xi^\star + K_D(\dot{\xi} - \dot{\xi}^\star)) + F_\xi^\star \tag{8a}$$
$$F_\theta(t) = -K_P(\theta - \theta^\star + K_D(\dot{\theta} - \dot{\theta}^\star)) + F_\theta^\star \tag{8b}$$

with K_D and K_P being the positive design parameters. As shown in [25], the control parameters can be tuned so that the closed-loop trajectory remains ϵ close to the robust reference maneuver, provided that the initial error and the uncertainty in μ are sufficiently small.

The main properties of the closed-loop system are detailed in the next proposition in which it is shown how, for an appropriate tuning of K_D and K_P, the actual closed-loop trajectory remains ϵ close to the robust reference maneuver, provided that the initial condition is sufficiently close to the reference and the uncertainty on μ is sufficiently small. In the statement of the proposition, we let $u = (F_1, F_2)$ and $\xi = (\xi, \dot{\xi}, \theta, \dot{\theta})$.

Proposition 1: Consider the closed-loop systems (2) and (8). There exist a $K_D^\star > 0$ and, for all positive $K_D \leq K_D^\star$, a $K_P^\star > 0$ such that for all $K_D \leq K_D^\star$ and $K_P \geq K_P^\star$,

there exist $\Delta_{\mathrm{TLs},0} > 0$ and $\Delta_{\mathrm{TLs},\mu} > 0$ such that if $\|\xi(t_0) - \xi^\star(t_0)\| < \Delta_{\mathrm{TLs},0}$ and $\|\mu - \mu_0\| \leq \Delta_{\mathrm{TLs},\mu}$, the following holds:

$$\|(\xi(t) - \xi^\star(t), u(t) - u^\star(t))\| < \epsilon \qquad \forall\, t \in [t_0, t_f].$$

For a proof, we refer the reader to [25].

3) Takeoff-and-Landing Controller: With $u^\star(t) = (F_1^\star(t), F_2^\star(t)) : [t_0, t_f] \to \mathbb{R}^2$ and $\xi^\star(t) = (\theta^\star(t), \dot\theta^\star(t)) : [t_0, t_f] \to \mathbb{R}^2$, a robust reference TL to LL transition maneuver, we define [see (3)]

$$F_\theta^\star(t) = (0 \quad 1)\, L(\theta^\star(t))^{-1} G(\theta^\star(t)) M \begin{pmatrix} F_1^\star(t) \\ F_2^\star(t) \end{pmatrix}$$

for all $t \in [t_0, t_f]$. The control law for the TL dynamics (5) is then chosen as

$$F_\theta = -K_P(\theta - \theta^\star + K_D(\dot\theta - \dot\theta^\star)) + F_\theta^\star \tag{9}$$

with K_D and K_P being the positive design parameters. The force inputs are computed using the restriction imposed by F_θ in the second row of (3) and the additional restriction

$$F_1(t) + F_2(t) = T_0 - v_T t$$

with T_0 being the initial thrust at the moment of the controller switch ($t = 0$) and $v_T > 0$. In [25], this control law is shown to be locally ISS with respect to uncertainty in the friction coefficient and to guarantee an error smaller then ϵ for sufficiently small uncertainties and initial error. This is detailed in the next proposition, which we reproduce for the sake of completeness, in which we let $u = (F_1, F_2)$ and $\xi = (\theta, \dot\theta)$.

Proposition 2: Consider the closed-loop system resulting from (5) and (9). Let $K_D > 0$. There exists a $K_P^\star > 0$ such that for all $K_P \geq K_P^\star$, there exist $\Delta_{\mathrm{TL},0} > 0$ and $\Delta_{\mathrm{TL},\mu} > 0$ such that if $\|\xi(t_0) - \xi^\star(t_0)\| < \Delta_{\mathrm{TL},0}$ and $\|\mu - \mu_0\| \leq \Delta_{\mathrm{TL},\mu}$, the following holds:

$$\|(\xi(t) - \xi^\star(t), u(t) - u^\star(t))\| < \epsilon \qquad \forall\, t \in [t_0, t_f].$$

4) Landed Mode: The landed state is the goal state of the landing maneuver. As such, in the operation mode the objective is to have the propellers of the vehicle come to a full halt, which is attained by setting both quadrotor forces to zero once the quadrotor is leveled with the landing slope, to prevent further movement. To avoid a large discontinuity in force input, we consider a maximum rate of variation for the propeller input and define the control law as

$$F_1(t) = \max(F_1(0) - \rho t, 0) \tag{10a}$$

$$F_2(t) = \max(F_2(0) - \rho t, 0) \tag{10b}$$

where the positive parameter ρ is the rate of variation of the thrust force.

C. Supervisor

The supervisor orchestrates the switching between the low-level controllers and feeds them with the appropriate reference maneuver according to the actual state of the vehicle. To apply the hybrid robust control strategy, we start by designing four robust reference maneuvers $(\xi_{\mathrm{FF}}^\star, u_{\mathrm{FF}}^\star) : [t_{01}, t_{f1}] \to \mathcal{D}(\mathrm{FF})$, $(\xi_{\mathrm{TLs}}^\star, u_{\mathrm{TLs}}^\star) : [t_{02}, t_{f2}] \to \mathcal{D}(\mathrm{TLs})$, $(\xi_{\mathrm{TL}}^\star, u_{\mathrm{TL}}^\star) : [t_{03}, t_{f3}] \to \mathcal{D}(\mathrm{TL})$, and $(\xi_{\mathrm{LL}}^\star, u_{\mathrm{LL}}^\star) : [t_{04}, t_{f4}] \to \mathcal{D}(\mathrm{LL})$ verifying the conditions detailed in Section III-A for some fixed ϵ and respective operative mode. Subsequently, with the reference maneuvers and ϵ fixed, we fix the four low-level controllers according to the structures and the design principles specified in Section III-B. Let u_{FF} be the FF controller and u_{TLs}, u_{TL}, and u_{LL} be the control laws discussed in Section III-B and expressed as (8), (9), and (10), respectively. The supervisor output switches the low-level controller according to the actual operating mode $q(t)$ of the vehicle. The latter takes value in the set {FF, TLs, TL, LL} and it is supposed to be known by combining measurements from sensors, either external or appropriately placed in the quadrotor airframe. The supervisor logic is thus simply $u(t) = u_{q(t)}(t)$.

We now detail the main properties achieved by the resulting closed-loop system that show how the desired landing maneuver takes place. The claims in the items immediately follow from joining the notion of robust reference maneuver and the properties of the low-level controllers highlighted in the propositions in Section III-B.

1) Let the exogenous disturbance δ be such that $\|\delta\|_\infty \leq \Delta_{\mathrm{FF},d}$ and let $\xi^\star(t_{01})$ and $\xi(t_{01})$ be such that $\|\xi(t_{01}) - \xi^\star(t_{01})\| \leq \Delta_{\mathrm{FF},0}$. Then there exists a time $t_{s1} \leq t_{f1}$ such that $q(t) = \mathrm{FF}$ for all $t \in [t_{01}, t_{s1})$ and $q(t_{s1}) = \mathrm{TLs}$. At time t_{s1}, the low-level controller is thus switched to u_{TLs}.
2) Let the uncertainties on the friction value be fulfilling $|\mu - \mu_0| \leq \Delta_{\mathrm{TLs},\mu}$ and let $\xi(t_{s1})$ and $\xi^\star(t_{02})$ be such that $\|\xi(t_{s1}) - \xi^\star(t_{02})\| \leq \Delta_{\mathrm{TLs},0}$ with $\Delta_{\mathrm{TLs},\mu}$ and $\Delta_{\mathrm{TLs},0}$ introduced in Proposition 1. Then there exists a time $t_{s2} \leq t_{s1} + t_{f2} - t_{02}$ such that $q(t) = \mathrm{TL}$ for all $t \in [t_{s1}, t_{s2})$ and $q(t_{s2}) = \mathrm{TL}$. At time t_{s3}, the low-level controller is thus switched to u_{TL}.
3) Let the uncertainties on the friction value be fulfilling $|\mu - \mu_0| \leq \Delta_{\mathrm{TL},\mu}$ with $\Delta_{\mathrm{TL},\mu}$ coming from Proposition 2. Then there exists a time $t_{s3} \leq t_{s2} + t_{f3} - t_{03}$ such that $q(t) = \mathrm{TLs}$ for all $t \in [t_{s2}, t_{s3})$ and $q(t_{s3}) = \mathrm{LL}$. At time t_{s3}, the low-level controller is thus switched to u_{LL}.
4) Let the controls $F_1(t)$ and $F_2(t)$ be set as (10). Then for all $t \in [t_{s3}, t_{s3} + t_{f4} - t_{04}]$, the vehicle stays robustly in the landed operating mode.

IV. Experimental Setup

To experimentally validate the proposed hybrid control architecture, we developed a rapid prototyping and testing architecture, using a MATLAB/Simulink environment to seamlessly integrate the sensors, the control algorithm, and the communication with the vehicle. The vehicle used for the experiments is a radio controlled Blade mQX quadrotor [28] shown in Fig. 7. This aerial vehicle is very agile and maneuverable, readily available, and inexpensive, making it the ideal platform for this paper.

The quadrotor weighs 80 g with battery included and the arm length from the CM to each of the motors is 11 cm. The available commands are thrust force and angular velocity. The maximum thrust generated by the propellers is approximately 1.37 N (equivalent to 140 g) and varies slightly with battery charge. The maximum angular velocity that can be

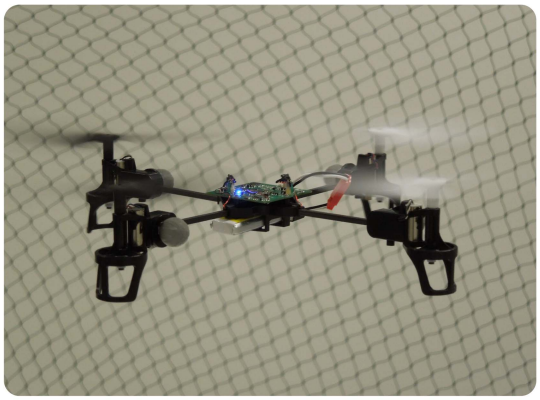

Fig. 7. Quadrotor platform.

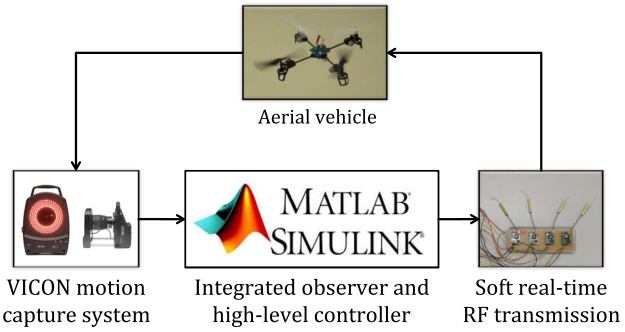

Fig. 8. Quadrotor control architecture.

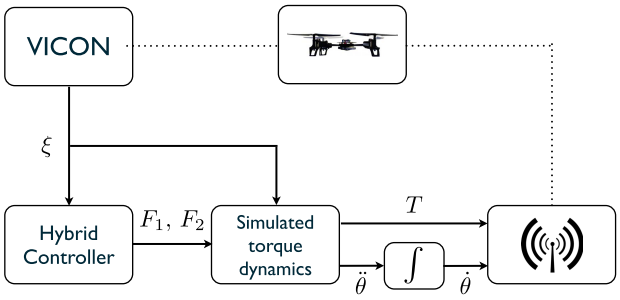

Fig. 9. Experimental setup with the simulated quadrotor state.

commanded is 200°/s for the x and y axes and 300°/s for the z-axis. However, the commands issued to the quadrotor are not instantaneously followed due to the inertia of the motors and general communication delays. The actuation dynamics can be well approximated by considering a first-order dynamic system, with a pole at 1.5 Hz, between the reference commands of thrust and angular velocity and the real inputs of the quadrotor.

Due to the lack of payload capability for on-board sensors, the state of the vehicle must be estimated through external sensors. In our setup, we use a VICON Bonita motion capture system [29], comprising 12 cameras, together with markers attached to the quadrotor. The motion capture system is able to accurately locate and estimate the positions of the markers, from which it obtains position and orientation measurements for the aircraft. VICON Bonita is a high performance system, able to operate with submillimeter precision at up to 120 Hz. The performance of the motion capture system is such that the linear velocity can be well estimated from the position measurements by a backward Euler difference, with a relatively low noise level. For the experimental setup, the state measurements from the motion capture system are obtained at 50 Hz, allowing for improved accuracy without compromising the bandwidth of the closed loop. The hybrid state of the vehicle is estimated from the vehicle state measurements with *a priori* knowledge of the landing strip location and slope. This can be interpreted as having a *virtual contact sensor* that establishes contact based on the distance information and is imbued with a small level of hysteresis. What is more, the switching logic relies only on contact information from that virtual contact sensor. For a quadrotor equipped with internal sensors, the hybrid state could be easily measured by placing contact sensors at the landing gear.

The vehicles are controlled by means of a 2.4-GHz wide-band direct-sequence spread spectrum signal that establishes a robust radio link with on-channel interference resistance. This radio technology also allows for the simultaneous use of several vehicles in a confined space, enabling formation flight. The commercial off-the-shelf quadrotor vehicles are designed to be human piloted with remote controls and not directly from a computer. To be able to send commands to a quadrotor from a computer, we identified the radio chip inside the remote control and connected the serial interface of the radio module to a computer serial port.

A schematic of the overall control architecture is presented in Fig. 8. We use two computer systems, the first running the VICON motion tracking software and the Simulink hybrid controller model, which generates command signals that are sent to the second computer through an Ethernet link; the second one receives the command signals and transmits them through the serial port to the radio module at the intervals of 22 ms. The decision to separate control and communications was made to avoid jitter in the transmission of the command signals to the radio module via the serial port, which occurred when running all the systems in the same computer and led to erratic communication with the vehicle.

V. Experimental Results

In this section, we present the results for an experimental run of the proposed hybrid controller. The inputs for the quadrotor used in this experiment do not include each motor force individually, thereby preventing the straightforward experimental testing of the theoretical framework. To overcome this issue, the $\ddot{\theta}$ dynamics are integrated in simulation using the appropriate dynamics (1), (2), (5), together with the inputs F_1 and F_2 coming from the low-level controllers. The resulting angular velocity $\dot{\theta}$ and the total thrust are then used as inputs for the physical quadrotor. This setup is shown in Fig. 9.

To adapt the physical setup to a 2-D control setting, the quadrotor is restricted to a vertical plane along the slope and its yaw is kept such that two of its landing gear contact points are aligned with the slope direction, as shown in Fig. 10. For the proposed maneuver, the quadrotor lands from the left to

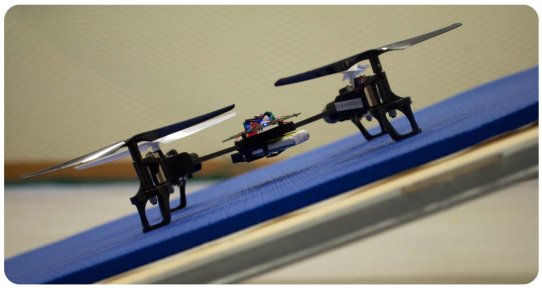

Fig. 10. Quadrotor aligned with the landing slope.

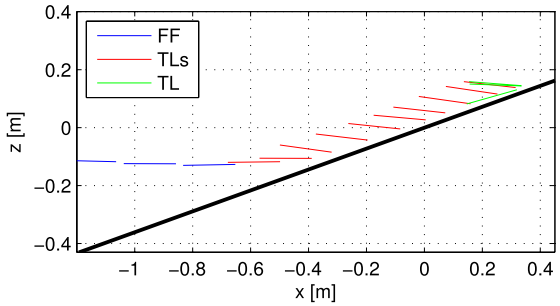

Fig. 11. Profile view of the complete quadrotor landing maneuver.

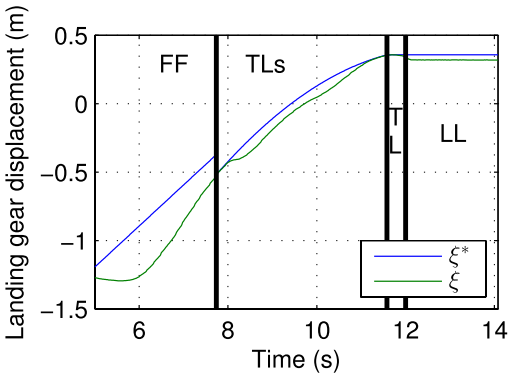

Fig. 12. Horizontal displacement along the slope.

the right, relative to Fig. 10, keeping the yaw angle such that both the right-side contact points touch the slope at the same time. Landing with a correct yaw angle allows the quadrotor to tilt and continue in the same plane, therefore satisfying the 2-D approximation.

The quadrotor's 2-D physical parameters are $l_g = r = 0.09$ m, $h_{\text{CM}} = 0.025$ m, $\ell = (l_g^2 + h_{\text{CM}}^2)^{1/2}$, and $\gamma = 15.5°$. The landing slope has a $\beta = 20°$ incline. The friction coefficient is taken as $\mu_0 = 1$. The controller design parameters are $K_{P\theta} = 3$, $K_{D\theta} = 0.2$, $K_{P\xi} = 0.2$, and $K_{D\xi} = 0.15$, for the TL and TLs mode local controllers.

For the landing procedure, the reference trajectory consists of a sequence of robust approach maneuvers FF $\rightarrow$ TLs, TLs $\rightarrow$ TL, and TL $\rightarrow$ LL, resulting in the vehicle sliding up the slope and coming to a halt at the desired landing point. The tracking of the quadrotor displacement and tilt angle is presented in Figs. 12 and 13. Figs. 12 and 13 are divided into four sections, corresponding to the four operation states transversed, with each one being labeled FF, TLs, TL, or LL

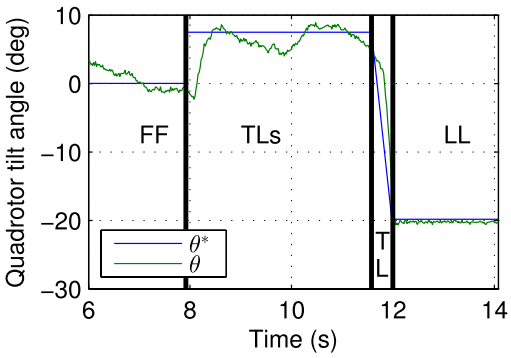

Fig. 13. Quadrotor tilt angle.

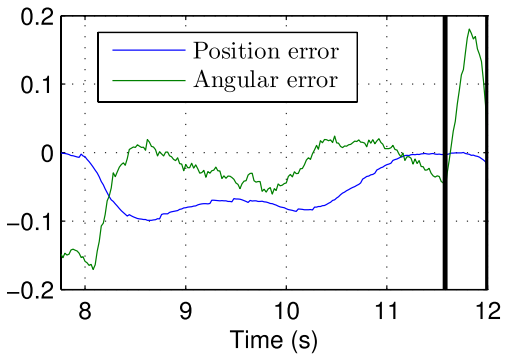

Fig. 14. Position and angular errors for the TLs and TL operating modes.

according to the respective operating mode. The transition to TLs occurs around 8 s, and at 11.5 s, the quadrotor stops sliding and enters the TL state. Finally, around 12 s, the quadrotor has two points of contact with the ground and enters the LL state, completing the landing procedure.

Observing Fig. 12, we can see the effects of the initial impact with the slope at the 8 s. The quadrotor starts an initial slide along the slope but looses velocity. This velocity is quickly recovered as the quadrotor tries to track the desired maneuver. Finally, the quadrotor comes to a halt and a transition to TL occurs, with the landed state being attained shortly afterward. Despite all the uncertainties existing in the model, the controller proves to be robust and maintains the tracking error small.

Looking at Fig. 13, we see the time evolution of the quadrotor's tilt angle. In FF, this angle is approximately zero, as asserted in the reference maneuver discussion in Section III-A1. Once in TLs, the quadrotor tracks a reference maneuver where $\theta_0 = 7.5°$. This tilt angle is close enough to the initial angle and confers increased controllability to the quadrotor. In addition, it helps to avoid a return to FF situation, as could happen easily if the reference maneuver was defined with $\theta_0 = 0$. Once the TL state is entered, the quadrotor tries to follow a constant angular velocity trajectory that leads to the complete contact of the landing gear with the landing slope.

A detailed view of the touch point position and quadrotor tilt angle errors can be observed in Fig. 14 for the TLs and TL operating modes. The absolute errors do not grow beyond 0.1 m for the position or 0.2 rad for the angle.

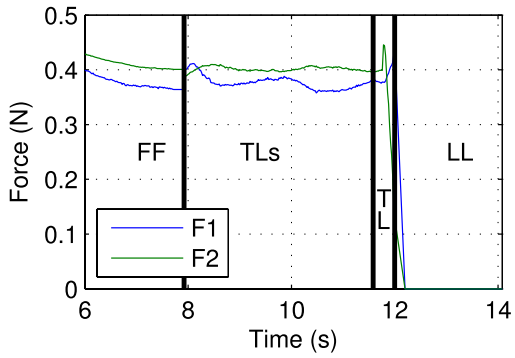

Fig. 15. Quadrotor forces generated by the propellers.

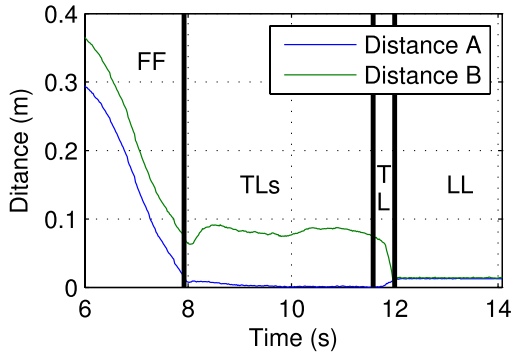

Fig. 16. Distance of the landing gear to the slope.

The evolution of the motor forces F_1 and F_2 throughout the maneuver is presented in Fig. 15. During the FF and TLs landing phases, the forces are similar in magnitude, reflecting a control of constant tilt angle. In TL, however, F_2 drops drastically, when forcing the rotation of the quadrotor and consequent landing. Nonetheless, F_1 and F_2 are always positive and within the limits of the quadrotor actuation.

The evolution of the distance of both landing gear extremities to the slope is shown in Fig. 16. In FF, both distances decrease at the same rate until contact with the ground happens at 8 s and the quadrotor enters the TLs state. After the transition, the contact point A [see Fig. 1(b)] remains on the slope for the duration of the maneuver. The contact point B on the landing gear gains a slight distance and then remains approximately constant, as the quadrotor tilts to track θ_0 and goes up the slope. Once in the TL operating mode, the distance of point B diminishes, as the quadrotor rotates, until both points are in contact with the landing slope. The distance is computed from the quadrotor position and attitude, knowing the slope's location and incline. The small resulting errors are due to imperfections in the landing slope surface.

Videos of the experimental results for the proposed landing maneuver and hybrid controller are available at [30].

VI. Conclusion

This paper addressed the problem of robust landing control of a quadrotor UAV, explicitly considering the interaction with the ground, which guarantees successful maneuvers even in sloped terrains and in the presence of external disturbances and uncertain parameters. The vehicle was modeled as a hybrid automaton, whose states reflect the different dynamic behaviors exhibited by the UAV along the stages of the landing maneuver. The landing procedure was then cast as the problem of changing the operating mode from the initial to the final desired state, through the edge transitions allowed for the hybrid automaton. The transitions between intermediate operating modes were achieved through the application of low-level feedback controllers, associated with each mode, to track robust reference signals. A supervisor controller was designed to sense the current operation mode of the vehicle and choose the appropriate low-level controller and corresponding robust reference trajectory. The combined properties of the low-level controllers and reference trajectories ensure that the desired intermediate transitions are attained, robustly with respect to uncertainties in the model and environment parameters, and that the final desired state is reached. The experimental results using a small-scale radio-controlled quadrotor vehicle were presented to assess the feasibility of the proposed hybrid controller, demonstrating the effectiveness of the proposed solution, especially for the cases in which the slope of the terrain renders the landing maneuver more demanding. Future work will be primarily focused on improvements to the hybrid dynamical model and the hybrid controller, toward having a vehicle that can operate resorting only to internal sensors. In particular, a complex integration of the sensors (contact and force) and avionics equipments will be required, extending the standard sensing capabilities of the vehicle to robustly detect the current operative mode. This latter issue also suggests the investigation of methodological solutions aiming at improving robustness to the possible uncertainties that may affect the measure of the current hybrid state.

References

[1] R. D. Braatz, "Unmanned aerial vehicles [about this issue]," *IEEE Control Syst.*, vol. 32, no. 5, pp. 8–9, Oct. 2012.
[2] C. Chen, B. M. Chen, and T. H. Lee, Eds., "Special issue on development of autonomous unmanned aerial vehicles," *Mechatronics*, vol. 21, no. 5, pp. 763–764, 2011.
[3] N. Michael, D. Scaramuzza, and V. Kumar, Eds., "Micro-UAV perception and control," *Auto. Robots*, vol. 33, nos. 1–2, pp. 1–214, Aug. 2012.
[4] K. P. Valavanis, Ed., "Special issue on unmanned aerial vehicles," *J. Intell. Robot. Syst.*, vol. 61, nos. 1–4, pp. 1–585, Jan. 2011.
[5] T. Hamel, R. Mahony, and A. Tayebi, Eds., "Aerial robotics [special issue]," *Control Eng. Pract.*, vol. 18, no. 7, pp. 677–836, Jul. 2010.
[6] G. Zhou, V. Ambrosia, A. J. Gasiewski, and G. Bland, "Foreword to the special issue on unmanned airborne vehicle (UAV) sensing systems for Earth observations," *IEEE Trans. Geosci. Remote Sens.*, vol. 47, no. 3, pp. 687–689, Mar. 2009.
[7] G. P. Martinsanz, Ed., "Unmanned aerial vehicles (UAVs) based remote sensing," *Remote Sens.*, vol. 4, no. 4, pp. 1090–3416, Apr. 2012.
[8] M.-D. Hua, T. Hamel, P. Morin, and C. Samson, "Introduction to feedback control of underactuated VTOL vehicles: A review of basic control design ideas and principles," *IEEE Control Syst.*, vol. 33, no. 1, pp. 61–75, Feb. 2013.
[9] J. M. Moore, "A system for landing an autonomous radio controlled helicopter on sloped terrain," M.S. thesis, Dept. Aeronautics Astron., Massachusetts Inst. Technol., Cambridge, MA, USA, 1994.
[10] B. Brogliato, *Nonsmooth Mechanics: Models, Dynamics and Control*. London, U.K.: Springer-Verlag, 1996.
[11] S. Bouabdallah and R. Siegwart, "Full control of a quadrotor," in *Proc. IEEE/RSJ Int. Conf. Intell. Robots Syst. (IROS)*, Oct./Nov. 2007, pp. 153–158.

[12] J. F. Roberts, T. S. Stirling, J.-C. Zufferey, and D. Floreano, "Quadrotor using minimal sensing for autonomous indoor flight," in *Proc. 3rd U.S.-Eur. Workshop Competition Micro-Aerial Vehicles, 7th Eur. Micro Air Vehicle Conf. Flight Competition*, 2007.
[13] L. Marconi, A. Isidori, and A. Serrani, "Autonomous vertical landing on an oscillating platform: An internal-model based approach," *Automatica*, vol. 38, no. 1, pp. 21–32, 2002.
[14] B. Herissé, T. Hamel, R. Mahony, and F.-X. Russotto, "Landing a VTOL unmanned aerial vehicle on a moving platform using optical flow," *IEEE Trans. Robot.*, vol. 28, no. 1, pp. 77–89, Feb. 2012.
[15] H. Voos and H. Bou-Ammar, "Nonlinear tracking and landing controller for quadrotor aerial robots," in *Proc. IEEE Int. Conf. Control Appl.*, Sep. 2010, pp. 2136–2141.
[16] D. Mellinger, M. Shomin, and V. Kumar, "Control of quadrotors for robust perching and landing," in *Proc. Int. Powered Lift Conf.*, 2010, pp. 205–225.
[17] A. L. Desbiens and M. R. Cutkosky, "Landing and perching on vertical surfaces with microspines for small unmanned air vehicles," *J. Intell. Robot. Syst.*, vol. 57, nos. 1–4, pp. 313–327, Jan. 2010.
[18] M. Fumagalli, R. Naldi, A. Macchelli, R. Carloni, S. Stramigioli, and L. Marconi, "Modeling and control of a flying robot for contact inspection," in *Proc. IEEE/RSJ Int. Conf. Intell. Robots Syst.*, Oct. 2012, pp. 3532–3537.
[19] L. Marconi and R. Naldi, "Control of aerial robots: Hybrid force and position feedback for a ducted fan," *IEEE Control Syst.*, vol. 32, no. 4, pp. 43–65, Aug. 2012.
[20] R. Goebel, R. G. Sanfelice, and A. Teel, "Hybrid dynamical systems," *IEEE Control Syst.*, vol. 29, no. 2, pp. 28–93, Apr. 2009.
[21] T. J. Koo, F. Hoffmann, H. Shim, B. Sinopoli, and S. Sastry, "Hybrid control of an autonomous helicopter," in *Proc. IFAC Workshop Motion Control*, 1998, pp. 285–290.
[22] E. Frazzoli, M. A. Dahleh, and E. Feron, "A hybrid control architecture for aggressive maneuvering of autonomous helicopters," in *Proc. 38th IEEE Conf. Decision Control*, vol. 3. Dec. 1999, pp. 2471–2476.
[23] J. H. Gillula, G. M. Hoffmann, H. Huang, M. P. Vitus, and C. J. Tomlin, "Applications of hybrid reachability analysis to robotic aerial vehicles," *Int. J. Robot. Res.*, vol. 30, no. 3, pp. 335–354, 2011.
[24] L. Marconi, R. Naldi, and L. Gentili, "Modelling and control of a flying robot interacting with the environment," *Automatica*, vol. 47, no. 12, pp. 2571–2583, 2011.
[25] D. Cabecinhas, R. Naldi, L. Marconi, C. Silvestre, and R. Cunha, "Robust take-off for a quadrotor vehicle," *IEEE Trans. Robot.*, vol. 28, no. 3, pp. 734–742, Jun. 2012.
[26] D. Cabecinhas, R. Naldi, L. Marconi, C. Silvestre, and R. Cunha, "Robust take-off and landing for a quadrotor vehicle," in *Proc. IEEE Int. Conf. Robot. Autom.*, May 2010, pp. 1630–1635.
[27] H. K. Khalil, *Nonlinear Systems*, 3rd ed. Englewood Cliffs, NJ, USA: Prentice-Hall, 2002.
[28] Horizon Hobby Inc. *Blade—#1 By Design*. [Online]. Available: http://www.bladehelis.com, accessed Jul. 24, 2015.
[29] VICON. *VICON Homepage*. [Online]. Available: http://www.vicon.com, accessed Jul. 24, 2015.
[30] *Video of the Landing Maneuver Hybrid Controller Experimental Results*. [Online]. Available: http://users.isr.ist.utl.pt/~dcabecinhas/landingmaneuver.m4v, accessed Jul. 24, 2015.

David Cabecinhas received the Licenciatura and Ph.D. degrees in electrical and computer engineering from the Instituto Superior Técnico, Lisbon, Portugal, in 2006 and 2014, respectively.

He has been a Researcher with the Laboratory of Robotics and Systems in Engineering and Science, Institute for Systems and Robotics, Lisbon, since 2007. He is currently a Post-Doctoral Fellow with the Faculty of Science and Technology, University of Macau, Macau, China. His current research interests include nonlinear control, sensor-based and vision-based control with applications to autonomous aerial and surface vehicles, and modeling and identification of aerial and surface vehicles.

Roberto Naldi received the Ph.D. degree in automation and operative research from the University of Bologna, Bologna, Italy, in 2008.

He is currently an Assistant Professor with the Department of Electrical, Electronic and Information Engineering, University of Bologna. His current research interests include nonlinear control, hybrid control with applications to aerial robotics, and modeling of small-scale aerial robots.

Carlos Silvestre received the Licenciatura degree in electrical engineering, the M.Sc. degree in electrical engineering, the Ph.D. degree in control science, and the Habilitation degree in electrical engineering and computers from the Instituto Superior Técnico (IST), Lisbon, Portugal, in 1987, 1991, 2000, and 2011, respectively.

He has been with the Department of Electrical Engineering, IST, since 2000, where he is currently an Associate Professor of Control and Robotics on leave. Over the past years, he has conducted research on the subjects of navigation guidance and control of air and underwater robots. He is a Professor with the Department of Electrical and Computers Engineering, Faculty of Science and Technology, University of Macau, Macau, China. His current research interests include linear and nonlinear control theory, coordinated control of multiple vehicles, gain scheduled control, integrated design of guidance and control systems, inertial navigation systems, and mission control and real time architectures for complex autonomous systems with applications to unmanned air and underwater vehicles.

Rita Cunha received the Licenciatura degree in information systems and computer engineering and the Ph.D. degree in electrical and computer engineering from the Instituto Superior Técnico (IST), Universidade de Lisboa, Lisbon, Portugal, in 1998 and 2007, respectively.

She is currently an Assistant Researcher with the Laboratory of Robotics and Systems in Engineering and Science, Institute for Systems and Robotics, Lisbon, and a Teaching Assistant with the Department of Electrical and Computer Engineering, IST. Her current research interests include nonlinear control, sensor-based control with applications to autonomous air vehicles, and modeling of small-scale helicopters and quadrotors.

Lorenzo Marconi received the Degree in electrical engineering from the University of Bologna, Bologna, Italy, in 1995.

He has held visiting positions with various research international institutions. He is currently a Professor with the University of Bologna. He has co-authored over 200 technical publications in linear and nonlinear feedback design in international journals, books, and conference proceedings. His current research interests include nonlinear control, output regulation, control of autonomous vehicles, fault detection and isolation, fault tolerant control.

Prof. Marconi received the Outstanding Application Paper Award from the International Federation of Automatic Control (IFAC) for a co-authored paper published in *Automatica* in 2005. He was a co-recipient of the 2014 *IEEE Control Systems Magazine* Outstanding Paper Award for the best paper in the magazine from 2012 to 2013. He is a member of the IEEE Control System Society and the Control System Society Conference Editorial Board. He is the Chair of the IFAC Technical Committee on Nonlinear Control Systems.